Neoplasia • Vol. 8, No. 5, May 2006, pp. 353–363 353

www.neoplasia.com

In Vivo Direct Molecular Imaging of Early Tumorigenesis and Malignant Progression Induced by Transgenic Expression of GFP–Met[1]

Sharon Moshitch-Moshkovitz, Galia Tsarfaty*,†, Dafna W. Kaufman*, Gideon Y. Stein‡, Keren Shichrur‡, Eddy Solomon‡, Robert H. Sigler*, James H. Resau*, George F. Vande Woude and Ilan Tsarfaty*,‡*

*Van Andel Research Institute, Grand Rapids, MI 49503, USA; †Sheba Medical Center, Diagnostic Imaging, Ramat Gan, Israel; ‡Department of Human Microbiology, Sackler School of Medicine, Tel Aviv University, Tel Aviv 69978, Israel

Abstract

The tyrosine kinase receptor Met and its ligand, hepatocyte growth factor/scatter factor (HGF/SF), play an important role in normal developmental processes, as well as in tumorigenicity and metastasis. We constructed a green fluorescent protein (GFP) Met chimeric molecule that functions similarly to the wild-type Met receptor and generated GFP–Met transgenic mice. These mice ubiquitously expressed GFP–Met in specific epithelial and endothelial cells and displayed enhanced GFP–Met fluorescence in sebaceous glands. Thirty-two percent of males spontaneously developed adenomas, adenocarcinomas, and angiosarcomas in their lower abdominal sebaceous glands. Approximately 70% of adenocarcinoma tumors metastasized to the kidneys, lungs, or liver. Quantitative subcellular-resolution intravital imaging revealed very high levels of GFP–Met in tumor lesions and in single isolated cells surrounding them, relative to normal sebaceous glands. These single cells preceded the formation of local and distal metastases. Higher GFP–Met levels correlated with earlier tumor onset and aggressiveness, further demonstrating the role of Met–HGF/SF signaling in cellular transformation and acquisition of invasive and metastatic phenotypes. Our novel mouse model and high-resolution intravital molecular imaging create a powerful tool that enables direct real-time molecular imaging of receptor expression and localization during primary events of tumorigenicity and metastasis at single-cell resolution.

Neoplasia (2006) **8,** 353–363

Keywords: Receptor tyrosine kinase, Met hepatocyte growth factor/scatter factor, sebaceous gland tumor, confocal intravital molecular imaging, GFP transgenic mice.

Introduction

The Met tyrosine kinase receptor and its ligand, hepatocyte growth factor/scatter factor (HGF/SF), are essential for embryonic development [1]. Met and HGF/SF are broadly expressed in adult tissues and have been implicated in the homeostasis of general physiological responses to tissue damage (including liver, kidney, and heart injuries) and in angiogenesis [1]. In addition, Met–HGF/SF signaling is involved in altering the metabolic activity of cells by enhancing both the glycolytic and the oxidative phosphorylation pathways [2,3].

Aberrant Met signaling has been widely implicated in most types of human cancers (http://www.vai.org/metandcancer). Met activation was also shown to play a role in the development of tumors expressing both epithelial and mesenchymal markers [4], and increased Met or HGF/SF expression often correlated with poor prognosis [5–8]. There are several ways by which Met can be activated in tumors: 1) autocrine signaling, as found in osteosarcoma and glioblastoma multiforme [9,10]; 2) paracrine signaling, as observed in carcinomas expressing Met, with HGF/SF being present in the stromal environment [1]; and 3) activation of *Met* mutations, which were originally discovered as germline mutations in families predisposed to several carcinomas [11] and recently found in a variety of cancers as sporadic mutations in the kinase, juxtamembrane, and extracellular domains [11,12].

Overexpression of both ligand and receptor is associated with several malignancies [13–15] and has been shown to be a strong independent predictor of recurrence, decreased survival [5,16–18], and poor prognosis [6,7] (http://www.vai.org/metandcancer). Met–HGF/SF signaling is also associated with malignant progression and metastasis of a large number of tumors, including human esophageal squamous cell carcinomas [19], prostate cancer [20], and ovarian cancer [21].

Met and HGF/SF display tumorigenic activity in a number of animal models. Transgenic Met expression in mice generates tumors such as hepatocellular carcinomas [22], whereas expression of mutationally activated Met receptors in transgenic and knockin mice leads to the onset of a wide range of tumors,

Address all correspondence to: Dr. Ilan Tsarfaty, Department of Human Microbiology, Sackler School of Medicine, Tel Aviv University, Tel Aviv 69978, Israel. E-mail: ilants@post.tau.ac.il

[1]This work was supported, in part, by a research grant from the National Institutes of Health (P50CA93990), a Breast Cancer Research Foundation grant, and by the Michigan Economic Development Corporation and the Michigan Technology Tri-Corridor (MAMC 085P1000815).

DOI 10.1593/neo.05634

including carcinomas and lymphomas [12,23]. Mice expressing an HGF/SF transgene in a tissue-specific manner display a wide variety of tumors, including melanomas, schwannomas, rhabdomyosarcomas, hepatomas, and mammary carcinomas [24,25], some of which develop metastases [26]. The tumors show high expression of the HGF/SF transgene and enhanced Met kinase activity. Overexpression of HGF/SF also induces severe developmental and functional abnormalities [24,27,28].

Recently, fluorescent proteins have been recruited into cancer research. Green fluorescent protein (GFP) has been used for detecting and tracking specific cancer cell lineages during tumor development [29–31] and has been coupled to proteins to follow their localization [32]. In this article, we describe a unique GFP–Met transgenic mouse model and a novel high-resolution intravital molecular imaging modality. Our results establish the first animal model that allows direct subcellular-resolution imaging of expression patterns of tyrosine kinase growth factor receptor in live animals. We show here that GFP–Met is responsible for the development of GFP–Met tumors and that following its expression enables the detection of transformed sebaceous glands and single cells outside the tumors that may be the precursors of local and distal metastases. Together, high-resolution imaging and our animal model may be used for studying the cellular and molecular mechanisms of tumorigenicity and metastasis, and for understanding the inhibitory effects and efficacy of Met-targeted cancer therapeutics *in vivo*.

Materials and Methods

Plasmid Construction and Generation of Transgenic Mice

The coding sequence of Met was amplified using the primers 5′-CGTAGGTACCATGAAGGCTCCCACC-GTGCTG-3′ and 5′-TAGTGGATCCGTGTTCCCCTCGC-CATCAAT-3′, which contain *Kpn*I and *Bam*HI restriction sites, respectively, at their 5′ ends. Met cDNA was cloned into the pEGFP-N1 vector (Clontech Laboratories, Mountain View, CA). To eliminate any mutations within the *Met* amplified coding region, a fragment of 3719 bp was digested out using *Bst*XI restriction enzyme and was replaced with a 3719-bp *Bst*XI fragment from pMB11 [33] to create pGFP–Met. The remaining amplified fragments were confirmed by sequencing. pGFP–Met plasmid was digested out of pGFP–Met, purified, and injected into mouse oocytes. GFP–Met transgenic founders were generated, as confirmed by polymerase chain reaction (PCR) analysis of the tail DNA. PCR amplification of GFP–Met was carried out using the following primers: 5′-TGTGCTCCTCTGGGAGCTCATGACGA-GAGG-3′ and 5′-CACTGCACGCCGTAGGTCAGGGTGGT-CACG-3′. Positive mice were identified by the amplification of a 0.5-kb DNA fragment. Experiments using mice were approved by the Van Andel Research Institute Institutional Animal Care and Use Committee.

Confocal Laser Scanning Microscopy (CLSM) Imaging

All confocal analyses were carried out using an LSM 510 META (Zeiss, Jena, Germany) confocal laser scanning microscope with the following configurations: 25-mW krypton/argon (488, 514, and 568 nm) and HeNe (633 nm) lasers, and a Ti-sapphire tunable pulse laser. To overcome the problem of high background fluorescence signals from an intact live mouse or an intact organ, spectral analysis was performed using a META detector. To isolate GFP fluorescence, lambda unmixing algorithm was used.

Intravital imaging of live mice was carried out using the above CLSM system. Mice were anesthetized with isoflurane (2.5% in oxygen), hair from the imaged area was removed using a depilatory cream, and the anesthetized mouse was placed on the microscope stage and kept anesthetized while being imaged. To avoid GFP signal reduction, frozen sections of different tissues were imaged unfixed using the META detector and the lambda unmixing algorithm.

Image analysis of average fluorescence intensity per square micrometer was carried out using MICA image analysis software (Cytoview LTD, Petach Tikva, Israel). The statistical difference in average area intensity in the different mice groups was calculated either by Student's *t* test or by analysis of variance using Microsoft Excel software (Microsoft, Redmond, WA).

Fluorescence-Activated Cell Sorter (FACS) Analysis

Blood samples were obtained by cardiac puncture. Samples were treated with red blood cell lysing buffer (R7757; Sigma-Aldrich, St. Louis, MO) in accordance with the manufacturer's instruction, washed thrice with phosphate-buffered saline (PBS), and subjected to FACS analysis.

Pathological Analyses

Tissues were immersion-fixed in neutral-buffered formalin overnight and processed in a graded series of solutions. Fixed tissues were dehydrated, embedded in paraffin, cut into 5-μm sections, and stained with hematoxylin and eosin (H&E). Histology and histopathology were characterized using standard anatomic pathology classifications and descriptions by two independent histopathologists. Diagnoses were recorded and incorporated into the data set for each animal and lesion.

Immunofluorescence Staining

Fixed sections were deparaffinized and blocked (5% bovine serum albumin and 10% normal donkey serum in PBS) for 30 minutes at room temperature. Slides were then incubated with anti-GFP antibody overnight at 4°C. After three washes in PBST (0.05% Tween 20 in PBS), cells were stained with either donkey anti-rabbit or anti-mouse antibody conjugated to either Texas Red or FITC (Jackson Immuno Research Laboratories, West Grove, PA) for 1 hour at room temperature in the dark. Slides were washed thrice in PBST and mounted with cover slips using GelMount (Biomeda, Foster City, CA). Immunostained sections were analyzed using the 510 Zeiss CLSM described above.

Western Blot (WB) Analysis and Immunoprecipitation (IP)

For biochemical experiments, tissues were homogenized in 0.4 ml of lysis buffer [20 mM Tris–HCl, pH 7.8, 100 mM

NaCl, 50 mM NaF, 1% NP40, 0.1% sodium dodecyl sulfate (SDS), 2 mM EDTA, and 10% glycerol] containing protease inhibitor cocktail (Roche Molecular Biochemicals, Mannheim, Germany) and 1 mM sodium orthovanadate. Cell lysates were clarified by centrifugation, and protein concentration was quantified using a BCA protein assay kit (Pierce, Rockford, IL). For IP, 500 μg of total protein was adjusted to a volume of 500 μl using a lysis buffer, and 5 μl of B_2 anti-Met monoclonal antibody (Santa Cruz Biotechnology, Santa Cruz, CA, USA) was added to each sample. Samples were incubated for 2 hours on ice, with occasional mixing. To precipitate antibody–Met complexes in the mixture, 50 μl of 50% protein G beads slurry (Amersham Biosciences, Uppsala, Sweden) was added to the mixture, and the samples were incubated in an inverting rotator for 2 hours at 4°C. The beads were then pelleted, washed thrice in a lysis buffer, and resuspended in 50 μl of 2× SDS loading buffer for gel electrophoresis. Samples were separated by SDS polyacrylamide gel electrophoresis and transferred onto a PVDF membrane (Invitrogen Life Technologies, Carlsbad, CA). Visualization was achieved using horseradish peroxidase–conjugated anti-mouse IgG, electrochemiluminescence reaction, and exposure to X-ray film (Kodak, Rochester, NY). On several occasions, the same membrane was subjected to several consecutive experiments following stripping with a fresh solution of Ponceau S (0.2% in 3% trichloroacetic acid in H_2O).

Ultrasound Analysis

Mice were monitored for tumor appearance once a week by palpation. Tumor size was measured by ultrasonography. Sonography was performed using a 15L8 linear transducer (15 MHz, Acuson Sequoia 512; Acuson, Mountain View, CA). Mice were anesthetized using isoflurane (oxygen flow, 1 l/min; isoflurane vaporizer up to 2%). Before sonography, hair in the tumor area was removed using a thin layer of Nair (Carter Product, New York, NY). A warm-water heating pad was used to avoid hypothermia during imaging. Gray-scale sonography was performed on days 0, 7, 14, and 21 after tumor palpation. Each animal was evaluated for tumor presence, size, and location. Imaging settings were standardized and were not changed throughout the experiment. No major near-field artifacts were encountered. Images were obtained by experienced sonographers who were blinded to the experiment. *In vivo* ultrasound experiments were performed in triplicate, showing similar results.

Results

pGFP–Met Construction and Activity

We generated a GFP–Met construct by fusing GFP to the C-terminus of murine met cDNA in the pGFP-N1 vector (pGFP–Met). To test GFP–Met expression, subcellular localization, and activation, we transiently transfected pGFP–Met into 293T cells and compared them to 293T cells transfected with mouse met. IP using anti-Met antibody, followed by immunoblotting (IB) with anti-Met antibody, displayed the classic 170- and 140-kDa mouse Met bands (Figure 1*A*) from 293T cells transfected with met, whereas GFP–Met–transfected cells displayed two bands at 200 and 170 kDa, which are the precursor and mature forms of GFP–Met, respectively, showing the additional 27 kDa of the GFP tag. Western blot analysis of pGFP–Met–transfected cells using anti-GFP antibodies revealed high levels of 200- and 170-kDa proteins (Figure 1*B*), whereas cells transfected with pGFP-N1 vector alone produced only a 27-kDa GFP band. These analyses validate that the 200- and 170-kDa proteins are GFP–Met.

Subcellular localization of GFP–Met was analyzed using the CLSM of transiently transfected 293T cells. GFP–Met signal was localized to the cell membrane (Figure 1*C*) in the pattern expected of an endogenous Met receptor [34]. Fluorescent signals were not detected in pMet-transfected 293T cells (Figure 1*D*), and GFP alone was distributed to the cytoplasm (data not shown).

We also tested whether GFP–Met retained endogenous biologic activities. GFP–Met activity was compared to Met activity in 293T transiently transfected cells. Cell lysates were subjected to IP with anti-Met and IB using anti–phosphorylated tyrosine (Figure 1*E*), anti–phosphatidyl inositol 3 kinase (PI3K) (Figure 1*F*), or anti-Grb2 (Figure 1*G*) antibodies. GFP–Met biologic function was retained in all tested signal transduction pathways. No significant decrease

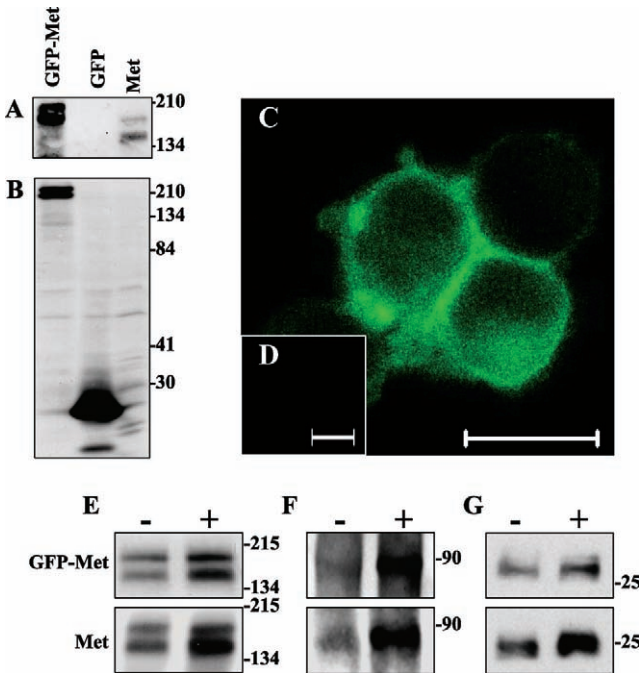

Figure 1. *GFP–Met retains Met biologic function and localization. The characterization of the transient expression of GFP–Met was carried out in 293T cells transiently transfected with pGFP–Met plasmids. Nontransfected, pMet-transfected, or pGFP-N1–transfected 293T cells served as controls. (A) IP and IB analyses of 293T cells transiently expressing GFP–Met, GFP, or Met using anti-GFP antibodies (IP) and anti-Met antibody (IB). (B) WB analysis of GFP–Met, GFP, and Met transient expression in 293T cells with anti-GFP antibody. CLSM fluorescence analysis of GFP–Met (C) and Met subcellular localization (D). Size bars, 20 μm. IP and IB analyses of 293T cells transiently expressing GFP–Met or Met in the presence (+) or absence (–) of HGF/SF. Cells were lysed and subjected to IP and WB analyses (E, F, & G). IP with anti-pTyr antibody and IB using anti-Met (E), IP with anti-Met and IB using anti-PI3K (F), or IP with anti-Met and IB using anti-Grb2 (G).*

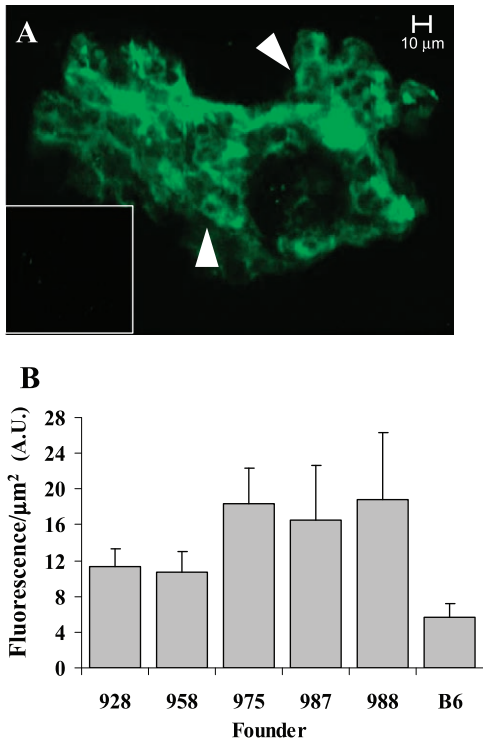

Figure 2. *GFP–Met transgenic expression in mice. (A) In vivo imaging of a sebaceous gland from a GFP–Met transgenic mouse. GFP–Met expression can be detected on the cell membrane of single cells in the gland (indicated by arrowheads). The inset shows an image from a nontransgenic mouse at the same conditions. Size bars, 20 μm. (B) Quantitative analysis of the fluorescence/area obtained from five different founder lines of GFP–Met transgenic mice. Each bar represents at least five mice (10 images per mouse).*

in its activity was observed, compared with Met. A minor effect on activity was observed in lower tyrosine phosphorylation levels on HGF/SF treatment (Figure 1*E*) and lower co-IP levels of both PI3K (Figure 1*F*) and Grb2 (Figure 1*G*). These results demonstrate that GFP–Met is biologically functional and that the GFP tag does not interfere with its signal transduction.

GFP–Met Expression in Transgenic Mice

We generated transgenic mice expressing GFP–Met from the CMV promoter using the pGFP–Met construct described above. Five founders were used in this study because differences between independent transgenic mouse lines and between different tissues expressing a reporter gene from the CMV promoter have been reported [35,36].

To image GFP–Met expression *in vivo*, we developed real-time high-resolution quantitative intravital molecular imaging using CLSM (see the Materials and Methods section). Imaging of transgenic mice revealed high expression levels of GFP–Met in sebaceous glands (Figure 2*A*). High levels of GFP–Met were observed on the cell membrane of sebaceous cells, revealing the overall three-dimensional structure of the gland at a very high resolution. Control nontransgenic mice showed only marginal background levels of green fluorescence (Figure 2*A*, *inset*). Quantitative analysis of fluorescence levels from 254 sebaceous glands showed variations between different founders (Figure 2*B*). Overall, GFP–Met transgenic mice showed *in vivo* higher fluorescence levels in their sebaceous glands relative to levels in the sebaceous glands of control nontransgenic mice. In three of the founder lines (975, 987, and 988), fluorescence was high; in two (928 and 958), fluorescence was moderate (Figure 2*B*) ($P = .0035$).

Analysis of GFP–Met expression in different organs shows high levels in the spleen, kidneys, and skin; moderate levels in the liver; low levels in the lungs; and marginal levels in the brain (data not shown), suggesting that GFP–Met is ubiquitously expressed in this transgenic mice model.

Overexpression of GFP–Met Induces Tumor Development in Transgenic Mice at an Early Age

GFP–Met transgenic male mice developed spontaneous tumors in the sebaceous glands of their lower abdominal skin area above the gonads (Figure 3*B*). The masses were not observed in female mice even at an older age (up to 2 years). Tumors were pale or red, round and lobular in appearance, and grew rapidly once they were palpable. The tumors were 0.5 to 0.8 cm in diameter when they ruptured, releasing sebaceous or pus-like sebum/liquid. Tumor development was observed in 32 ± 3.6% of male mice (Figure 3*A*, *gray bars*) at an average age of 6.9 ± 3.01 months (Figure 3*B*, *white bars*). Tumor onset was detected between 1.5 and 16 months of age. Early tumor onset positively correlated with GFP–Met expression levels (Figure 3*A*). Founder lines with high GFP–Met expression (975, 987, and 988) developed tumors earlier than lines with moderate expression (928 and 958) (average age of 6.1 and 10.7 months, respectively; $P = .0015$).

To substantiate the hypothesis that tumor development in the sebaceous gland correlates with high levels of GFP–Met, we performed comparative intravital CLSM analyses of normal and transformed sebaceous glands. Intravital optical molecular imaging of sebaceous glands in the lower abdominal area revealed increased expression levels in transformed sebaceous glands ($n = 11$) compared with normal glands of both male and female mice ($n = 23$ and $n = 21$, respectively; Figure 3*C*). GFP–Met levels were 1.83 times higher in neoplastic glands than in normal male sebaceous glands, and were 1.78 times higher ($P = 2.33 \times 10^{-11}$) in male than in female transgene sebaceous glands of the distal ventral abdominal area. These results further demonstrate a positive correlation between high GFP–Met levels and tumorigenic phenotype.

Pathological analyses of GFP–Met tumors revealed hyperproliferative sebaceous gland tumors that were identified mainly as adenomas, adenocarcinomas, and angiosarcomas (Figure 3*D*). H&E staining of the secreted material revealed no cells but a puss-like degraded necrotic substance (data not shown).

Control transgenic mice, expressing only GFP from a tie-2 promoter, demonstrated a wide range of tissue expressions, including those in the sebaceous glands (data not shown). However, no phenotype was evident, suggesting that GFP itself is not responsible for tumor formation in the sebaceous glands in GFP–Met transgenic mice.

Imaging Early Events of Metastasis

Intravital optical molecular imaging of tumor areas revealed single cells spreading from the tumor and expressing high GFP–Met levels (Figure 4, *A* and *B*) relative to surrounding normal tissues. Such single cells were not detected around normal sebaceous glands (data not shown). To further monitor GFP–Met expression in sebaceous gland tumors, CLSM of excised and frozen tumor sections was performed. Close examination of intact excised tumors revealed single cells expressing high levels of GFP–Met in patches on the cell surface (Figure 4*C*). Imaging of unfixed frozen sections of tumors revealed a large number of cells

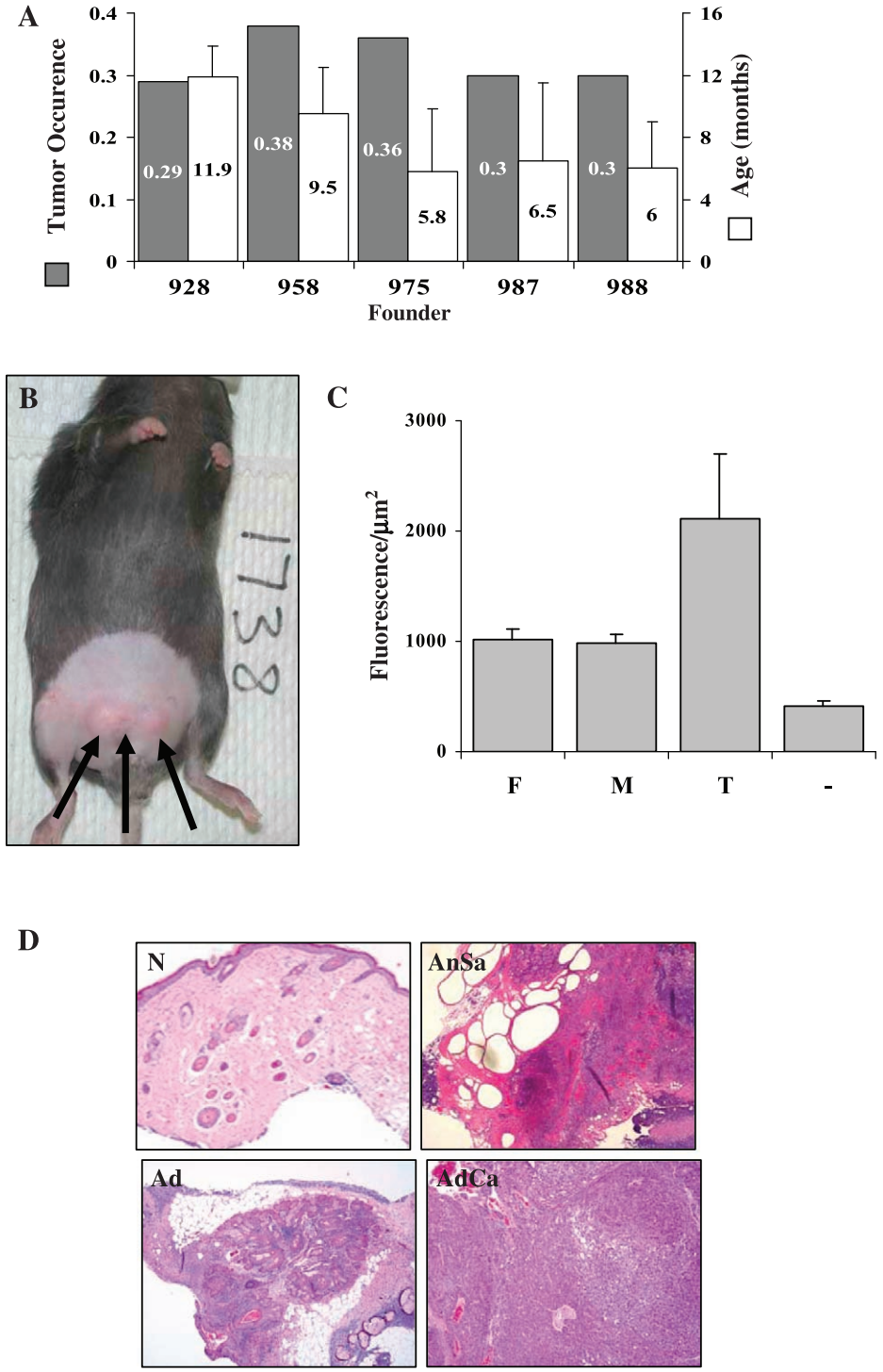

Figure 3. *Male GFP–Met transgenic mice develop sebaceous gland tumors. (A) Tumor occurrence rate (dark bars) and age of tumor onset (white bars) according to founder lines (928, 958, 975, 987, and 988; n = 22, 21, 91, 50, and 63, respectively). (B) Sebaceous gland tumors spontaneously develop in the lower abdominal area of male GFP–Met transgenic mice. (C) Quantitative analysis of the fluorescence/area of normal sebaceous glands obtained from males and females (M and F, respectively) relative to transformed (T) glands. Each bar represents at least five mice (10 images per mouse). (D) H&E staining of sebaceous gland tumors: normal skin (N), adenoma (Ad), angiosarcoma (AnSa), and adenocarcinoma (AdCa).*

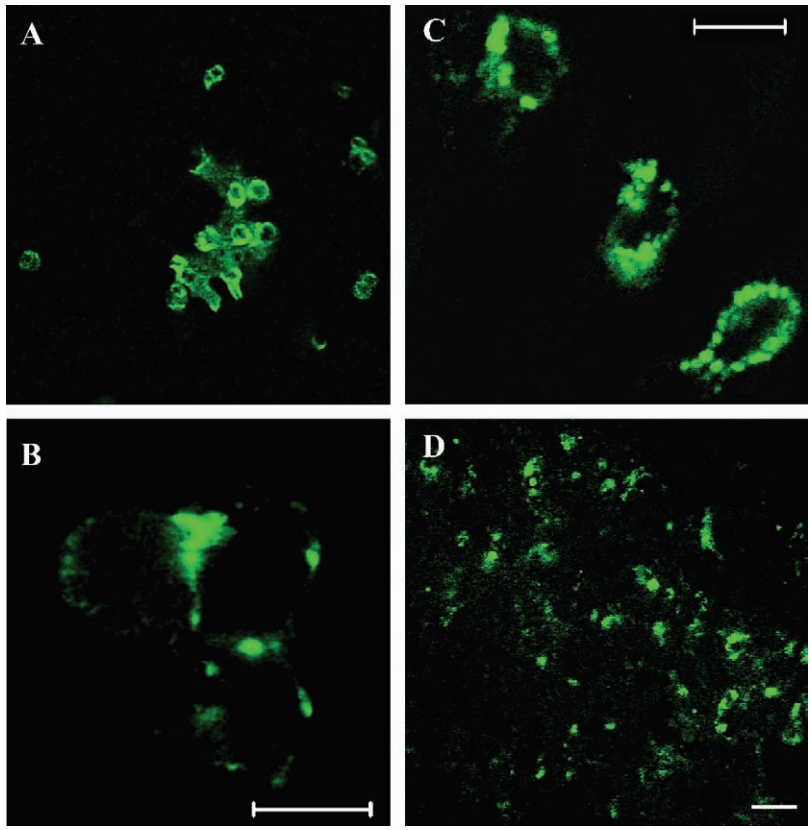

Figure 4. *Imaging single cells expressing GFP–Met. Single cells expressing high levels of GFP–Met could be detected in close proximity to the tumor by intravital imaging at low (A) and high (B) magnifications. Single cells expressing high levels of GFP–Met in patches on their cell surface were also imaged in excised intact tumors (C), as well as in unfixed frozen sections of sebaceous gland adenocarcinomas (D). Size bars, 20 μm.*

overexpressing GFP–Met (Figure 4*D*). These cells were absent in frozen sections of normal tissues (data not shown).

Transgenic GFP–Met mice harboring tumors with or without metastasis were screened for single metastatic cells with high fluorescence in their blood, using FACS analysis of 1×10^6 cells after red blood cells lysis (see Materials and Methods section). GFP–Met mice that did not develop tumors served as negative controls. Single cells expressing high levels of GFP–Met were isolated from blood samples of mice harboring a tumor and demonstrating metastasis (1371 per 1×10^6 cells). A significantly lower number was obtained from GFP–Met tumor-bearing mice that did not develop metastasis (481 per 1×10^6 cells), and only 210 fluorescent cells were counted in mice not harboring tumors. A detailed analysis of the cells' fluorescence levels revealed that cells originating from mice harboring a tumor and demonstrating metastasis exhibited high fluorescence levels (data not shown), whereas cells originating from mice without a tumor demonstrated significantly lower fluorescence levels. Confocal microscope analysis of the cells showed a typical membrane-bound GFP–Met fluorescence. Cells obtained from mice bearing primary tumors showed only moderate levels of fluorescence in the blood. These results indicate that single cells expressing high levels of GFP–Met could be detected *in vivo*, in excised tumors, and in the blood of mice bearing tumors and demonstrating metastases.

Immunohistochemical analysis of fixed GFP–Met tumors and their margins was carried out using anti-GFP antibodies. GFP–Met staining was strong in tumor regions, with increased levels in peripheral areas (Figure 5, *A* and *C*). Normal skin tissues surrounding the tumor showed only marginal GFP–Met levels. Within tumor margins, single cells expressing high levels of the receptor were detected (Figure 5, *A* and *C*). Close examination of H&E staining (Figure 5*B*) revealed that these cells had prominent nuclei and relatively abundant amphiphilic cytoplasm consistent with anaplastic or neoplastic alterations. These individual cells appear morphologically similar to GFP–Met tumor cells (Figure 5*B*). We were also able to detect local micrometastases of GFP–Met tumors (Figure 5*C*). H&E staining of the area revealed a clump of cells that are plumper and more amphiphilic than surrounding mesenchymal cells, suggesting that these cells have altered growth consistent with neoplasia (Figure 5*D*). Vascularization adjacent to this cell clump is evident in H&E staining. Importantly, GFP–Met molecular imaging allowed the identification of these metastatic cells in what was analyzed as normal surrounding tissues in H&E sections (Figure 5, *B* and *D*). This finding further supports the observation made by others that tissues surrounding a primary tumor commonly contain transformed cells with metastatic potential [37].

In addition, we compared the fluorescence levels of tumor cells, normal cells, and single metastatic cells in tumor

margins from four different mice. Tumor cells and single metastatic cells appeared to exhibit similar high florescence levels (4.3- and 3.4-fold, respectively) compared with normal tissue fluorescence (normalized to 1.0), suggesting that these highly fluorescent cells are single metastatic cells.

Follow-Up of Tumor Development in GFP–Met Transgenic Mice

Tumor size and anatomic progression were followed *in vivo* by ultrasound imaging. Tumors were imaged weekly starting at the early stages of tumor palpation. GFP–Met tumors grew rapidly from 180 to 270 mm^3 (Figure 6*A*, *a* and *b*) and then ruptured, resulting in decreased size (144 mm^3; Figure 6*Ac*), followed by the observation of local metastases in close proximity to the original tumor (Figure 6*Ad*). Single cells that were detected by CLSM around the tumor (Figure 5) may be the precursors of these local metastases. Pathological analysis was performed on 40 mice. The majority of tumors were malignant and were identified as adenocarcinomas (42.5%), angiosarcomas (27.5%), or poorly differentiated nonidentified tumors (10%); the minority (20%) were benign adenomas (Figure 6*B*). Thirty-five percent of GFP–Met transgenic mice that developed tumors also developed metastases. Metastases were found locally in the skin and in distant organs such as the liver, lungs, and kidneys. Pathological analyses revealed sebaceous gland adenocarcinoma morphology in 70.6% of metastases and angiosarcomas in 18.2% of metastases (Figure 6*B*).

Biochemical analysis of the levels of GFP–Met precursor (p200) and processed (p170) forms was performed in normal and transformed sebaceous glands (Figure 6*C*). GFP–Met levels increase gradually from low in normal skin, to moderate in adenoma and angiosarcoma, and to high in adenocarcinoma—the most aggressive tumor in our model (70.6% of metastases). These results demonstrate a positive correlation between GFP–Met levels and tumor aggression.

To further validate the high GFP–Met levels observed in tumors relative to normal sebaceous glands, we performed immunostaining on multiple sections of normal and sebaceous gland tumors (33 and 31 sections, respectively) in a GFP–Met tissue array using anti-GFP antibody. GFP–Met expression level was significantly elevated in the tumors (Figure 7, *C* and *D*) relative to normal skin (Figure 7, *A* and *B*). Quantitative analysis of fluorescence levels, normalized per area, was performed (Figure 7*E*; $n = 64$, $P = 8.6 \times 10^{-12}$). The average GFP–Met level in tumors appeared to be three times higher than the average level in normal skin samples of the same mice. Similar results were obtained with anti-pTyr antibody. A 2.72-fold increase in tyrosine phosphorylation was observed in tumors relative to normal tissues (data not shown), indicating that Met and its substrates are phosphorylated and activated. To avoid misinterpretation of results, fluorescence levels were measured in normal sebaceous glands and tumor areas only, defined as a region of interest in the MICA image analysis software. Our results indicate significantly higher GFP–Met levels in

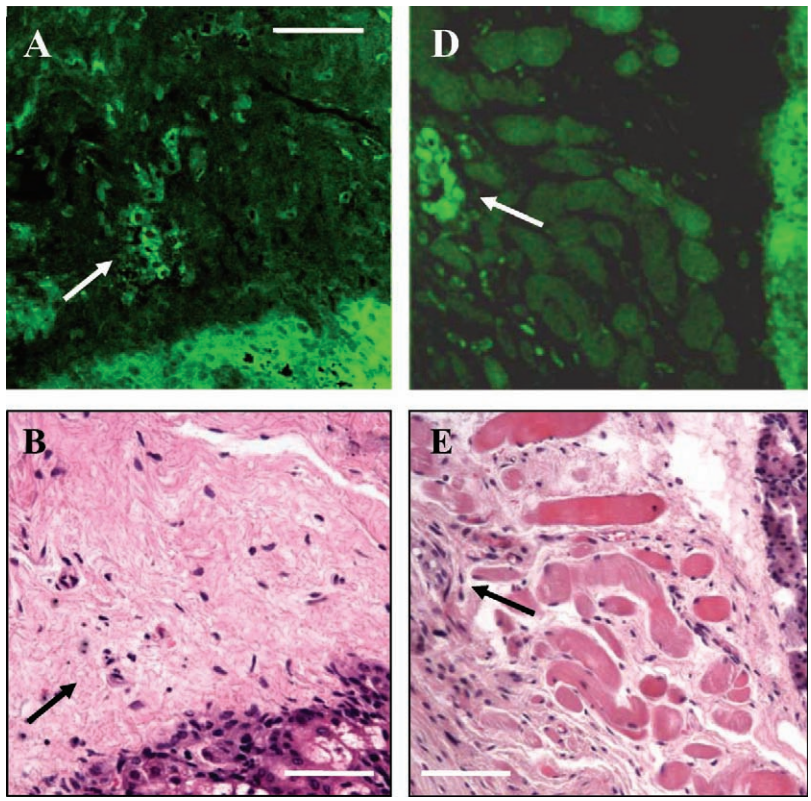

Figure 5. *Imaging tumor margins. Immunostaining with anti-GFP antibody and H&E staining of fixed adenocarcinoma sections. (A) Immunostaining of single cells expressing high levels of GFP–Met in tumor margins. (B) H&E staining of the same area shown in (A). An arrow marks single cells in the two sections. (D) Immunostaining of micrometastasis in tumor margins. (E) H&E staining of the same area shown in (D). Arrows indicate the area with single cells/micrometastasis expressing high levels of GFP–Met. Size bars, 50 μm.*

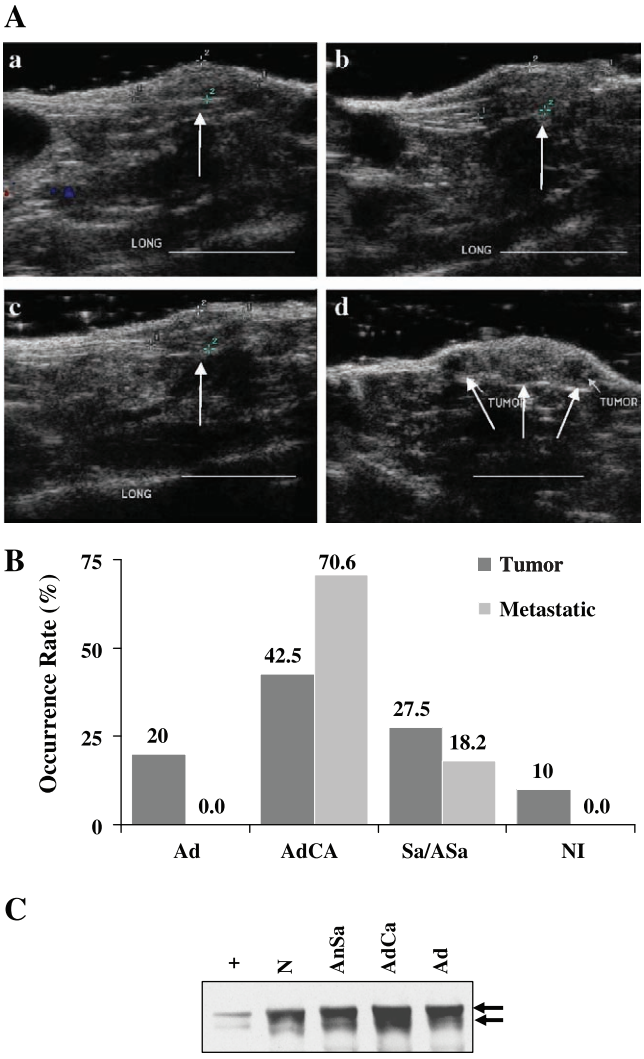

Figure 6. *GFP–Met sebaceous gland tumor progression. (A) Sebaceous gland tumors were monitored weekly (a–d) using ultrasound imaging. Tumor size was measured. Two new local metastases developed on week 4 (d). Tumors are indicated by arrows. Size bars, 1 cm. (B) Histopathology of the tumors revealed them to be adenomas (Ad), adenocarcinomas (AdCa), a combination of adenomas and adenocarcinomas (AdCa + Ad), angiosarcomas (AnSa), or poorly developed nonidentified (NI) tumors. The percentage of each subtype is shown by gray bars; the percentage of metastatic tumors is shown by open bars. Thirty-five percent of the tumors also develop metastases; most of those were identified as adenocarcinomas. (C) WB analysis of GFP–Met IP from homogenized tissue cell lysates of normal skin (N), adenoma (Ad), adenocarcinoma (AdCa), and angiosarcoma (AnSa). A cell lysate of pGFP–Met–transformed 293T cells serves as a positive control (+). GFP–Met levels increase gradually from low in normal skin, to moderate in adenoma and angiosarcoma, to high in adenocarcinoma.*

tumor cells than in normal sebaceous gland cells, further demonstrating the major role of Met in tumorigenesis.

Discussion

Aberrant Met–HGF/SF–Met signaling plays a significant role in the pathogenesis of many types of solid tumors and other malignancies. The abnormal expression of Met and HGF/SF in most types of human cancer is associated with poor clinical outcome [1]. To better understand the primary events of tumorigenesis and metastasis, we have used transgenic mice, in combination with molecular imaging, as our model system. In this study, we show that transgenic mice expressing GFP–Met develop distinct neoplasms in male murine sebaceous glands. These tumors developed in all five independent transgenic lines and included adenoma, adenocarcinoma, and angiosarcoma histopathology. Some malignant lesions developed metastases to the lungs, kidneys, and liver. Spontaneous occurrence of sebaceous tumors, as observed in our animals, is rare in wild-type mice. We have shown that GFP–Met levels are higher in transformed sebaceous glands and that there is a positive correlation between GFP–Met levels and both age of tumor onset and tumor aggressiveness. Our results strongly suggest that, in this transgenic model, tumors developed as a direct effect of high GFP–Met expression levels, indicating that these high levels are essential for tumor development. GFP is not responsible for this spontaneous tumor development because transgenic GFP expression in mice did not yield any sebaceous gland tumor. This is consistent with other works in which a number of GFP-expressing transgenic mice have been produced with no reported malignant phenotype [38–41]. Higher expression levels of Met in the tumors were not observed in Met transgenic breast cancer models [42]. Our results clearly demonstrate that higher levels of GFP–Met produce cellular circumstances that support tumor development.

Met overexpression in breast cancer has been reported in a large number of studies [1]. A positive correlation between Met levels and tumor aggressiveness on patients was demonstrated in primary breast cancers and their lymph node metastases. High Met levels in node-positive breast cancer patients correlated with poor clinical outcome, independent of Her2/neu [8]. Our results here further validate Met overexpression in human malignancies as an important player in tumorigenesis and metastasis. In this study, we observed higher levels of GFP–Met expression in tumor tissues relative to corresponding normal tissues. Previous studies have shown that increased Met levels could result either from transcriptional upregulation or from increased protein stabilization. Elevated met mRNA levels, accompanied by increased protein levels, have been reported in human lung adenocarcinoma cells [43] and human breast tumors [44]. However, because GFP–Met is driven by the CMV promoter rather than the endogenous Met promoter, it is reasonable to assume that higher GFP–Met levels in the tumor are due to protein stabilization. The ubiquitin–proteasome pathway is known to play a significant role in Met degradation and may be important for averting cellular transformation [12]. In the future, protein turnover in normal and tumor tissues will be examined to determine the basis of increased GFP–Met tumor levels.

The gradual increase in GFP–Met levels from normal skin, to adenoma and angiosarcoma, to adenocarcinoma, as demonstrated here, correlates with tumor progression. We hypothesize that, during the physiological development of sebaceous glands, cells expressing high GFP–Met levels propagate and form foci of transformed cells within the gland.

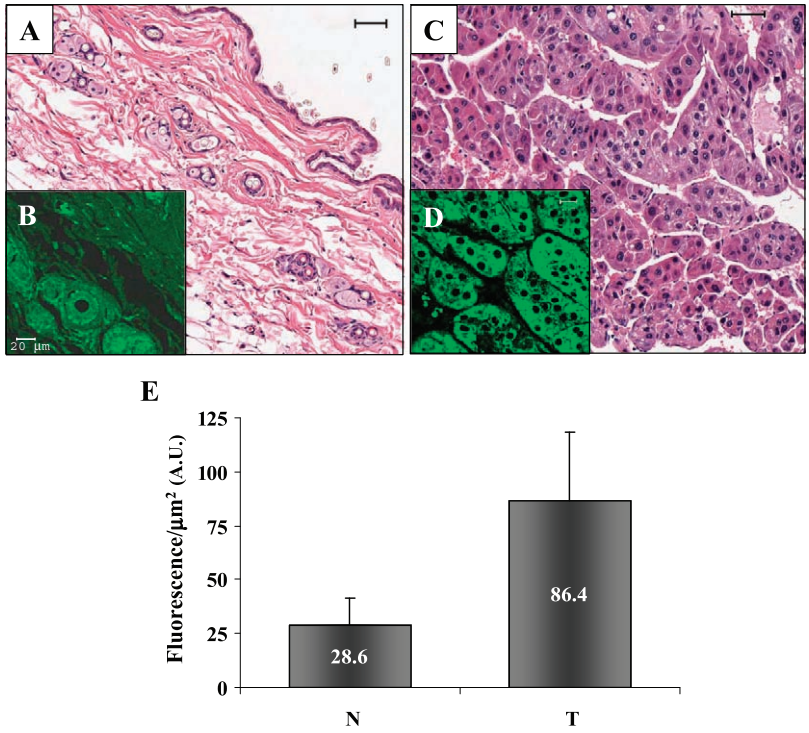

Figure 7. *GFP–Met expression in normal skin and sebaceous gland tumors. GFP–Met levels were assessed in tumor and normal sections by immunostaining using anti-GFP antibody. (A) H&E staining of normal skin. Size bar, 50 μm. (B) Immunostaining of normal GFP–Met mouse skin from (A). Size bar, 20 μm. (C) H&E staining of GFP–Met sebaceous gland adenocarcinoma. Size bar, 50 μm. (D) Immunostaining of the tumor in (C). Size bar, 20 μm. (E) Quantitative analysis of GFP–Met normal and tumor expressions from normal and tumor samples ($P = 8.6 \times 10^{-12}$). N, normal sebaceous glands; T, tumors.*

Gender and organ specificity of tumor development were observed in all five GFP–Met founder lines independently. The molecular mechanisms underlying this specificity are not fully understood. A paracrine loop between stromal compartments of the hair follicle (expressing HGF/SF) [45] and GFP–Met in adjacent sebaceous glands may contribute to organ specificity. The involvement of androgens in GFP–Met tumor development, resulting from crosstalk between Met–HGF/SF signaling and androgen receptor–testosterone complexes, has been already suggested in several studies [46–48]. Crosstalk between androgen- and HGF/SF-activated signaling pathways is considered to be the result of interactions between transcription factors that regulate gene expression, resulting in a synergistic effect in the growth stimulation of prostate epithelial cells [49]. The development of sebaceous gland tumors adjacent to the male gonads suggests that sex hormone dependency may play a role in this animal model, particularly because there is a 25% incidence of sebaceous carcinomas in the region of the external genitalia [50]. The role of androgen involvement and gender specificity will be further studied in our laboratory.

GFP–Met–induced sebaceous tumors raise the question of the possible involvement of Met in human sebaceous gland tumors. As in our model, human neoplasms of the sebaceous glands may be benign (sebaceous hyperplasia or sebaceous gland adenomas) or malignant. Malignant human sebaceous gland carcinomas also have organ preference and are common in the head and neck, but mostly in the eyelids (75%). These tumors tend to grow in nests with central necrosis, resembling the appearance of GFP–Met tumors. Similarly, they produce both local and distal metastases. In addition, histopathological analyses reveal strong similarity between these mouse and human malignancies. In contrast to the GFP–Met mouse model, women (67%) have a higher occurrence rate of sebaceous gland carcinomas than men (http://www.emedicine.com/oph/topic716.htm). The role of Met in human sebaceous gland carcinoma has not been studied, and the molecular mechanisms involved in human sebaceous gland transformation are not clear, except for overexpression of nuclear p53 and expression of c-erbB-2 oncoprotein in a small number of cases [51,52]. Taken together, these results show that our transgenic mice may serve as an animal model for studying human sebaceous gland carcinoma.

Tumor metastasis is a highly selective process that involves a large number of regulatory mechanisms. The process begins with the detachment of cells from the primary tumor by disruption of cell–cell interactions, which permits the migration of tumor cells away from the primary tumor [53]. Successful formation of metastases also requires angiogenesis in the primary tumor site, followed by increased tumor cell motility, which results in invasion into the new vessels and tumor cell embolism [54]. The role of HGF/SF in reducing the aggregation of tumor cells and in facilitating dissociation and scattering has been demonstrated in breast carcinoma and other malignancies [55]. To elude apoptotic elimination, neoplastic cells must display a versatile set of adhesive receptors by either expression or functional activation

of integrins. Upregulation of integrin transcription, as well as integrin aggregation and activation, was demonstrated to be induced by Met–HGF/SF signaling [55]. In addition, matrix metalloproteases (MMPs), which localize and concentrate matrix digestion at sites of directional cell invasion, can selectively cleave extracellular matrix components to facilitate cell migration [56]. HGF/SF plays an important role in the regulation of MMP-mediated proteolysis by both enhancing the transcriptional levels of a large number of MMPs and stimulating the conversion of their precursor forms into active enzymes [55]. We describe the imaging of single cells that express high levels of GFP–Met and spread from the tumor. We hypothesize that these single cells are early precursors of the metastasis of GFP–Met tumors.

In this paper, we present a novel approach for imaging the early events of tumorigenesis and metastasis by using high-resolution intravital optical molecular imaging to detect and follow GFP–Met expression. An important benefit of molecular imaging assays is their quantitative nature, as well as their ability to depict three-dimensional information regarding the spatial distribution of a particular protein in a particular cell/organ or throughout the entire body in a living animal [57]. Here, we demonstrate the ability of confocal intravital molecular imaging to directly detect and quantify tyrosine kinase receptor expression at subcellular resolution.

Our results establish GFP–Met transgenic mice as the first animal model to enable direct single-cell resolution imaging of tyrosine kinase growth factor receptor expression patterns in a live animal. Such high-resolution modalities may be crucial for understanding the cellular and molecular mechanisms of tumorigenicity and metastasis, and for evaluating inhibitory mechanisms and the efficacy of cancer therapeutics in preclinical trials.

References

[1] Birchmeier C, Birchmeier W, Gherardi E, and Woude GV (2003). Met, metastasis, motility and more. *Nat Rev Mol Cell Biol* **4** (12), 915–925.

[2] Yerushalmi GM, Leibowitz-Amit R, Shaharabany M, and Tsarfaty I (2002). Met–HGF/SF signal transduction induces mimp, a novel mitochondrial carrier homologue, which leads to mitochondrial depolarization. *Neoplasia* **4** (6), 510–522.

[3] Kaplan O, Firon M, Vivi A, Navon G, and Tsarfaty I (2000). HGF/SF activates glycolysis and oxidative phosphorylation in DA3 murine mammary cancer cells. *Neoplasia* **2** (4), 365–377.

[4] Tsarfaty I, Rong S, Resau JH, Rulong S, da Silva PP, and Vande Woude GF (1994). The *Met* proto-oncogene mesenchymal to epithelial cell conversion. *Science* **263** (5143), 98–101.

[5] Tsarfaty I, Alvord WG, Resau JH, Altstock RT, Lidereau R, Bieche I, Bertrand F, Horev J, Klabansky RL, Keydar I, et al. (1999). Alteration of *met* protooncogene product expression and prognosis in breast carcinomas. *Anal Quant Cytol Histol* **21** (5), 397–408.

[6] Qian CN, Guo X, Cao B, Kort EJ, Lee CC, Chen J, Wang LM, Mai WY, Min HQ, Hong MH, et al. (2002). Met protein expression level correlates with survival in patients with late-stage nasopharyngeal carcinoma. *Cancer Res* **62** (2), 589–596.

[7] Ma P, Takashi K, Maulik G, Fox E, Sattler M, Griffin J, Johnson B, and Salgia R (2003). C-MET mutational analysis in small cell lung cancer: novel juxtamembrane. *Cancer Res* **63** (19), 6272–6281.

[8] Lengyel E, Prechtel D, Resau JH, Gauger K, Welk A, Lindemann K, Salanti G, Richter T, Knudsen B, Vande Woude GF, et al. (2005). C-Met overexpression in node-positive breast cancer identifies patients with poor clinical outcome independent of Her2/neu. *Int J Cancer* **113** (4), 678–682.

[9] Koochekpour S, Jeffers M, Rulong S, Taylor G, Klineberg E, Hudson EA, Resau JH, and Vande Woude GF (1997). Met and hepatocyte growth factor/scatter factor expression in human gliomas. *Cancer Res* **57** (23), 5391–5398.

[10] Fukuda T, Ichimura E, Shinozaki T, Sano T, Kashiwabara K, Oyama T, Nakajima T, and Nakamura T (1998). Coexpression of HGF and c-Met/HGF receptor in human bone and soft tissue tumors. *Pathol Int* **48** (10), 757–762.

[11] Schmidt L, Duh FM, Chen F, Kishida T, Glenn G, Choyke P, Scherer SW, Zhuang Z, Lubensky I, Dean M, et al. (1997). Germline and somatic mutations in the tyrosine kinase domain of the *MET* proto-oncogene in papillary renal carcinomas. *Nat Genet* **16** (1), 68–73.

[12] Jeffers M, Fiscella M, Webb CP, Anver M, Koochekpour S, and Vande Woude GF (1998). The mutationally activated Met receptor mediates motility and metastasis. *Proc Natl Acad Sci USA* **95** (24), 14417–14422.

[13] Jin L, Fuchs A, Schnitt SJ, Yao Y, Joseph A, Lamszus K, Park M, Goldberg ID, and Rosen EM (1997). Expression of scatter factor and c-met receptor in benign and malignant breast tissue. *Cancer* **79** (4), 749–760.

[14] Rong S, Oskarsson M, Faletto D, Tsarfaty I, Resau JH, Nakamura T, Rosen E, Hopkins RFd, and Vande Woude GF (1993). Tumorigenesis induced by coexpression of human hepatocyte growth factor and the human *met* protooncogene leads to high levels of expression of the ligand and receptor. *Cell Growth Differ* **4** (7), 563–569.

[15] Kang JY, Dolled-Filhart M, Ocal IT, Singh B, Lin CY, Dickson RB, Rimm DL, and Camp RL (2003). Tissue microarray analysis of hepatocyte growth factor/Met pathway components reveals a role for Met, matriptase, and hepatocyte growth factor activator inhibitor 1 in the progression of node-negative breast cancer. *Cancer Res* **63** (5), 1101–1105.

[16] Yamashita J, Ogawa M, Yamashita S, Nomura K, Kuramoto M, Saishoji T, and Shin S (1994). Immunoreactive hepatocyte growth factor is a strong and independent predictor of recurrence and survival in human breast cancer. *Cancer Res* **54** (7), 1630–1633.

[17] Ghoussoub RA, Dillon DA, D'Aquila T, Rimm EB, Fearon ER, and Rimm DL (1998). Expression of c-met is a strong independent prognostic factor in breast carcinoma. *Cancer* **82** (8), 1513–1520.

[18] Altstock RT, Stein GY, Resau JH, and Tsarfaty I (2000). Algorithms for quantitation of protein expression variation in normal *versus* tumor tissue as a prognostic factor in cancer: *Met* oncogene expression, and breast cancer as a model. *Cytometry* **41** (3), 155–165.

[19] Ren Y, Cao B, Law S, Xie Y, Lee PY, Cheung L, Chen Y, Huang X, Chan HM, Zhao P, et al. (2005). Hepatocyte growth factor promotes cancer cell migration and angiogenic factors expression: a prognostic marker of human esophageal squamous cell carcinomas. *Clin Cancer Res* **11** (17), 6190–6197.

[20] MacDougall CA, Vargas M, Soares CR, Holzer RG, Ide AE, and Jorcyk CL (2005). Involvement of HGF/SF–Met signaling in prostate adenocarcinoma cells: evidence for alternative mechanisms leading to a metastatic phenotype in Pr-14c. *Prostate* **64** (2), 139–148.

[21] Wong AS, Roskelley CD, Pelech S, Miller D, Leung PC, and Auersperg N (2004). Progressive changes in Met-dependent signaling in a human ovarian surface epithelial model of malignant transformation. *Exp Cell Res* **299** (1), 248–256.

[22] Wang R, Ferrell LD, Faouzi S, Maher JJ, and Bishop JM (2001). Activation of the Met receptor by cell attachment induces and sustains hepatocellular carcinomas in transgenic mice. *J Cell Biol* **153** (5), 1023–1034.

[23] Graveel C, Su Y, Koeman J, Wang LM, Tessarollo L, Fiscella M, Birchmeier C, Swiatek P, Bronson R, and Vande Woude G (2004). Activating *Met* mutations produce unique tumor profiles in mice with selective duplication of the mutant allele. *Proc Natl Acad Sci USA* **101** (49), 17198–17203.

[24] Takayama H, LaRochelle W, Sharp R, Otsuka T, Kriebel P, Anver M, Aaronson S, and Merlino G (1997). Diverse tumorigenesis associated with aberrant development in mice. *Proc Natl Acad Sci USA* **94** (2), 701–706.

[25] Bell A, Chen Q, DeFrances MC, Michalopoulos GK, and Zarnegar R (1999). The five amino acid–deleted isoform of hepatocyte growth factor promotes carcinogenesis in transgenic mice. *Oncogene* **18** (4), 887–895.

[26] Gallego MI, Bierie B, and Hennighausen L (2003). Targeted expression of HGF/SF in mouse mammary epithelium leads to metastatic adenosquamous carcinomas through the activation of multiple signal transduction pathways. *Oncogene* **22** (52), 8498–8508.

[27] Otsuka T, Takayama H, Sharp R, Celli G, LaRochelle W, Ilmore NE, Vieira W, Owens JW, Anver M, and Merlino G (1998). C-Met autocrine activation induces development of malignant melanoma and. *Cancer Res* **58** (22), 5157–5167.

[28] Sakata H, Takayama H, Sharp R, Rubin JS, Merlino G, and LaRochelle WJ (1996). Hepatocyte growth factor/scatter factor overexpression induces growth, abnormal development, and tumor formation in transgenic mouse livers. *Cell Growth Differ* **7** (11), 1513–1523.

[29] Wack S, Hajri A, Heisel F, Sowinska M, Berger C, Whelan M, Marescaux J, and Aprahamian M (2003). Feasibility, sensitivity, and reliability of laser-induced fluorescence imaging of green fluorescent protein–expressing tumors *in vivo*. *Mol Ther* **7** (6), 765–773.

[30] Nakanishi H, Mochizuki Y, Kodera Y, Ito S, Yamamura Y, Ito K, Akiyama S, Nakao A, and Tatematsu M (2003). Chemosensitivity of peritoneal micrometastases as evaluated using a green fluorescence protein (GFP)–tagged human gastric cancer cell line. *Cancer Sci* **94** (1), 112–118.

[31] Steinbauer M, Guba M, Cernaianu G, Kohl G, Cetto M, Kunz-Schughart LA, Geissler EK, Falk W, and Jauch KW (2003). GFP-transfected tumor cells are useful in examining early metastasis *in vivo*, but immune reaction precludes long-term tumor development studies in immunocompetent mice. *Clin Exp Metastasis* **20** (2), 135–141.

[32] Pepperkok R, Simpson JC, and Wiemann S (2001). Being in the right location at the right time. *Genome Biol* **2** (9): REVIEWS1024.

[33] Rong S, Bodescot M, Blair D, Dunn J, Nakamura T, Mizuno K, Park M, Chan A, Aaronson S, and Vande Woude GF (1992). Tumorigenicity of the *met* proto-oncogene and the gene for hepatocyte growth factor. *Mol Cell Biol* **12** (11), 5152–5158.

[34] Faletto DL, Tsarfaty I, Kmiecik TE, Gonzatti M, Suzuki T, and Vande Woude GF (1992). Evidence for non-covalent clusters of the c-*met* proto-oncogene product. *Oncogene* **7** (6), 1149–1157.

[35] Sawicki JA, Morris RJ, Monks B, Sakai K, and Miyazaki J-I (1998). A composite CMV-IE enhancer/[beta]-actin promoter is ubiquitously expressed in mouse cutaneous epithelium. *Exp Cell Res* **244** (1), 367–369.

[36] Schmidt EV, Christoph G, Zeller R, and Leder P (1990). The cytomegalovirus enhancer: a pan-active control element in transgenic mice. *Mol Cell Biol* **10** (8), 4406–4411.

[37] Yokoyama N, Shirai Y, Ajioka Y, Nagakura S, Suda T, and Hatakeyama K (2002). Immunohistochemically detected hepatic micrometastases predict a high risk of intrahepatic recurrence after resection of colorectal carcinoma liver metastases. *Cancer* **94** (6), 1642–1647.

[38] Okabe M, Ikawa M, Kominami K, Nakanishi T, and Nishimune Y (1997). ''Green mice'' as a source of ubiquitous green cells. *FEBS Lett* **407** (3), 313–319.

[39] Villuendas G, Gutierrez-Adan A, Jimenez A, Rojo C, Roldan ER, and Pintado B (2001). CMV-driven expression of green fluorescent protein (GFP) in male germ cells of transgenic mice and its effect on fertility. *Int J Androl* **24** (5), 300–305.

[40] Hadjantonakis AK and Nagy A (2001). The color of mice: in the light of GFP-variant reporters. *Histochem Cell Biol* **115** (1), 49–58.

[41] Ahmed F, Wyckoff J, Lin EY, Wang W, Wang Y, Hennighausen L, Miyazaki J, Jones J, Pollard JW, Condeelis JS, et al. (2002). GFP expression in the mammary gland for imaging of mammary tumor cells in transgenic mice. *Cancer Res* **62** (24), 7166–7169.

[42] Muller WJ (1991). Expression of activated oncogenes in the murine mammary gland: transgenic models for human breast cancer. *Cancer Metastasis Rev* **10** (3), 217–227.

[43] Boccaccio C, Gaudino G, Gambarotta G, Galimi F, and Comoglio PM (1994). Hepatocyte growth factor (HGF) receptor expression is inducible and is part of the delayed–early response to HGF. *J Biol Chem* **269** (17), 12846–12851.

[44] Parr C, Watkins G, Mansel RE, and Jiang WG (2004). The hepatocyte growth factor regulatory factors in human breast cancer. *Clin Cancer Res* **10** (1 Pt 1), 202–211.

[45] Lindner G, Menrad A, Gherardi E, Merlino G, Welker P, Handjiski B, Roloff B, and Paus R (2000). Involvement of hepatocyte growth factor/scatter factor and met receptor signaling in hair follicle morphogenesis and cycling. *FASEB J* **14** (2), 319–332.

[46] Nakashiro K, Hara S, Shinohara Y, Oyasu M, Kawamata H, Shintani S, Hamakawa H, and Oyasu R (2004). Phenotypic switch from paracrine to autocrine role of hepatocyte growth factor in an androgen-independent human prostatic carcinoma cell line, CWR22R. *Am J Pathol* **165** (2), 533–540.

[47] Sirotnak FM, She Y, Khokhar NZ, Hayes P, Gerald W, and Scher HI (2004). Microarray analysis of prostate cancer progression to reduced androgen dependence: studies in unique models contrasts early and late molecular events. *Mol Carcinog* **41** (3), 150–163.

[48] Seol DW and Zarnegar R (1998). Structural and functional characterization of the mouse c-*met* proto-oncogene (hepatocyte growth factor receptor) promoter. *Biochim Biophys Acta* **1395** (3), 252–258.

[49] Sasaki M and Enami J (1999). Mammary fibroblast–derived hepatocyte growth factor and mammogenic hormones stimulate the growth of mouse mammary epithelial cells in primary culture. *Endocr J* **46** (3), 359–366.

[50] DeVita V, Hellman S, and Rosenberg S (2001). *Cancer Principles and Practice of Oncology*. Lippincott Williams and Wilkins, Philadelphia, PA. 1994.

[51] Gonzalez-Fernandez F, Kaltreider SA, Patnaik BD, Retief JD, Bao Y, Newman S, Stoler MH, and Levine PA (1998). Sebaceous carcinoma. Tumor progression through mutational inactivation of p53. *Ophthalmology* **105** (3), 497–506.

[52] Hasebe T, Mukai K, Ishihara K, Kaneko A, and Shimosato Y (1992). Sebaceous gland and sweat gland carcinomas of the skin. Clinicopathological study and significance of c-erbB-2 oncoprotein expression. *Acta Pathol Jpn* **42** (8), 585–594.

[53] Fidler IJ (2002). The organ microenvironment and cancer metastasis. *Differentiation* **70** (9–10), 498–505.

[54] Li CY, Shan S, Cao Y, and Dewhirst MW (2000). Role of incipient angiogenesis in cancer metastasis. *Cancer Metastasis Rev* **19** (1–2), 7–11.

[55] Trusolino L and Comoglio PM (2002). Scatter-factor and semaphorin receptors: cell signalling for invasive growth. *Nat Rev Cancer* **2** (4), 289–300.

[56] Wang H and Keiser JA (2000). Hepatocyte growth factor enhances MMP activity in human endothelial cells. *Biochem Biophys Res Commun* **272** (3), 900–905.

[57] Itoh J, Serizawa A, Kawai K, Ishii Y, Teramoto A, and Osamura RY (2003). Vascular networks and endothelial cells in the rat experimental pituitary glands and in the human pituitary adenomas. *Microsc Res Tech* **60** (2), 231–235.